Published in final edited form as:
Nat Neurosci. 2014 September ; 17(9): 1208–1216. doi:10.1038/nn.3760.

Independent control of gamma and theta activity by distinct interneuron networks in the olfactory bulb

Izumi Fukunaga[1,3,*], **Jan Herb**[1,2,3], **Mihaly Kollo**[1,3], **Edward S Boyden**[5], and **Andreas T Schaefer**[1,2,3,4,*]

[1]Behavioural Neurophysiology, Max-Planck-Institute for Medical Research

[2]Dept Anatomy & Cell Biology, Faculty of Medicine, University of Heidelberg, Germany

[3]Division of Neurophysiology, MRC National Institute for Medical Research

[4]Dept of Neuroscience, Physiology & Pharmacology, University College London, UK

[5]Media Lab, Synthetic Neurobiology Group, Massachusetts Institute of Technology, Cambridge MA, USA

Abstract

Circuits in the brain possess a remarkable ability to orchestrate activities on different timescales, but how distinct circuits interact to sculpt diverse rhythms remains unresolved. The olfactory bulb is a classic example where slow, theta, and fast, gamma, rhythms coexist. Furthermore inhibitory interneurons generally implicated in rhythm generation are segregated into distinct layers, neatly separating local from global motifs. Here, combining intracellular recordings in vivo with circuit-specific optogenetic interference we dissect the contribution of inhibition to rhythmic activity in the mouse olfactory bulb. We found that the two inhibitory circuits control rhythms on distinct timescales: local, glomerular networks coordinate theta activity, regulating baseline and odor-evoked inhibition; granule cells orchestrate gamma synchrony and spike timing. Surprisingly, they did not contribute to baseline rhythms, or sniff-coupled odor-evoked inhibition despite their perceived dominance. Thus, activities on theta and gamma time scales are controlled by separate, dissociable inhibitory networks in the olfactory bulb.

Temporal structure is an essential aspect of communication in the brain. This is particularly evident in olfaction, where neural representations are defined by sniffing[1], animals are able to distinguish stimuli arriving at precise times within a sniff cycle[2], and evidence for timing sensitivities in higher olfactory regions are beginning to emerge[3]. Given the importance of inhibitory circuits in neural computation, they are likely to play crucial roles in shaping such temporal structures in a wide range of frequencies[4-8]. Interplays of inhibitory and excitatory neurons are thought to underlie synchronous activities at fast, gamma frequencies[4,5], as well

*Correspondence to: ifukuna@nimr.mrc.ac.ukaschaef@nimr.mrc.ac.uk.

Author contributions I.F. and A.T.S conceived and designed the experiments and wrote the paper with inputs from all authors. I.F. performed in vivo experiments in anesthetized and awake animals. J.T.H. performed in vitro physiology experiments and made and characterized AAV. M.K. contributed data from awake animals. E.S.B. provided ArchT viral constructs and assisted with design of the optogenetic experiments.

Europe PMC Funders Author Manuscripts

as on slower, theta time scales[7]. While modeling studies[4] and *in vitro* recordings[8] often predict circuit properties underlying rhythm generation, demonstrations of direct causal links *in vivo* remain scarce[5,6]. In addition, mechanisms underlying oscillations within a particular band are often studied in isolation, yet activities on different timescales coexist during many brain functions[9]; both slow and fast rhythms are expressed by the same individual principal neurons[9], interneuron activities show distinct phase relations to slow and fast rhythms simultaneously[7], and the same molecularly defined interneuron class is for example implicated in driving gamma oscillations[5] as well as setting theta phase[6]. Thus, it is not clear if common mechanisms govern both timescales or if indeed circuits underlying slow and fast activity might be dissociable. Experimental dissection of these hypotheses *in vivo* faces particular challenges, largely because specific interneurons involved in generating and coordinating different rhythms are often found overlapping anatomically as well as molecularly[7,8].

The mammalian olfactory bulb (OB) provides a unique advantage in such quests. Here, two key classes of inhibitory circuits are anatomically segregated (Supplementary Fig. 1a), making dissection of circuits contributing to temporal structuring potentially feasible. The dynamics in the OB are characterized by activities spanning several distinct time scales, most notably in slow theta (1-12 Hz, refs[10,11]; Supplementary Fig. 1b,c) and fast gamma (40-100 Hz, refs[4,10,11]; Supplementary Fig. 1d) band activities. The former primarily arises from olfactory inputs robustly locking to the sniff rhythm[1,12-18]. However, even in the absence of odorous stimuli, distinct classes of projection neurons lock to different respiration phases[15-17] (Supplementary Fig. 1b). It is inhibition in the OB that causes this temporal segregation[16], where one class of projection neurons, mitral cells (MCs), is delayed relative to the other, tufted cells (TCs). Previous reports linked granule cells (GCs) to a role in shaping respiration coupling of projection neurons as these interneurons exhibit robust sniff locking[14,17-19]. Recent computational work in turn postulated glomerular feedforward circuitry as an underlying mechanism[16]. In addition to the baseline rhythm, odor presentations often evoke a variety of activities in the theta range[10,12-14,18,20], notably inhibitory responses (Supplementary Fig. 1c). Such inhibitory responses are implicated in contrast enhancement and are widely thought to be mediated by lateral inhibition via GCs[19-21] although more recent computational work propose alternative explanations based on feedforward inhibition[22]. Theta rhythms in turn provide a framework to the latter, fast, gamma-range activities generated in the OB, which occur nested in sniff rhythms[10] (Supplementary Fig. 1d). Such fast activities are observed under various behavioural states[10,23] and are correlated with higher task demands[10,23]. It is evident from pharmacological studies *in vitro* and *in vivo* that $GABA_A$ mediated inhibition is a basis for gamma activity[24,25]. Modeling[26], current-source density analysis[10] as well as localized pharmacology in brain slices[24] and constitutive genetic alteration of GC excitation[27] have pointed towards a prominent contribution from GCs to gamma activity, yet conclusive evidence is lacking so far.

Thus, while inhibition is clearly implicated in defining both gamma and theta range activities, the specific circuits behind the variety of temporal structures in the OB remain largely enigmatic. Here we used whole-cell recordings from interneurons and projection

neurons and LFP recordings in the OB in brain slices, in anaesthetized and awake mice in combination with pharmacological and circuit-specific optogenetic interference to dissect the contribution of GC and glomerular layer interneurons to gamma and theta activity in the OB.

Results

Efficient and selective silencing of interneurons in the OB

MCs and TCs both tightly lock to distinct but opposite phases of the sniff cycle, whose shift is established by inhibition in the OB[16]. To assess the circuits underlying this phase segregation, we aimed to selectively silence interneurons in the GC layer (GCL) or glomerular layer *in vivo*. We first assessed the efficiency and selectivity of optogenetic silencing using GCL injections (Fig. 1). We injected adeno-associated virus (AAV 1/2) for conditional expression of the photo-activatable proton pump, archaerhodopsinT (ArchT, ref [28]) into transgenic animals expressing Cre recombinase from an IRES construct in the Gad2- or Vgat-loci[29,30], aiming to restrict silencing to GABAergic neurons (Fig. 1a). 58% of GCL neurons are reported to express GAD2[31]. While no such report exists for VGAT expression, virtually all GABAergic neurons are thought to express VGAT[30]. With our deep, GCL injections, more than 90% of Cre expressing neurons in the GCL also expressed the fluorescently tagged ArchT (90.2 ± 2.4 %, n = 8 slices; Fig 1a). To assess the extent and specificity of silencing we performed whole-cell recordings from GCs and MCs in brain slices solely under IR guidance for blind sampling. Consistent with the expected Cre-expression rate, 29 out of 49 (59%) GCs in slices from Gad2-Cre animals hyperpolarized by more than 10 mV upon white light presentations (Fig. 1c). In slices from Vgat-Cre animals, 22 of 26 GCs hyperpolarized by more than 10 mV, corresponding to efficient silencing of 85% of GCs *in vitro* (Fig. 1d). *In vivo*, blind whole-cell recordings from GCs mirrored the *in vitro* results: in Gad2-Cre animals with GCL injection, 50% (9 out of 18 cells) of GCs hyperpolarized by more than 10 mV upon light stimulation (Fig. 1e). Average evoked hyperpolarisation for such infected cells was −20.4 ± 2.4 mV (Fig. 1f). In Vgat-Cre animals this rate was 87% (13/15 cells, Fig. 2h). Notably, GCs consistently hyperpolarized by more than 20 mV at depths 800 μm below the brain surface (Supplementary Fig. 2). Importantly, excitatory odor responses evoked in GCs were consistently and completely suppressed (3/3 responses, Fig. 1g-i).

Deep injections resulted in infection highly restricted to the GCL: judged by immunohistochemistry, less than 2% of all infected neurons (1.57 ± 1.8 %, n = 3 slices) were located outside the GCL, in the glomerular or external plexiform layers. In addition, recordings from 151 MCs *in vitro* from Gad2-Cre animals with GCL injection showed no hyperpolarization upon light stimulation (Fig. 1b), indicating indeed infection is specific to Cre-expressing neurons (also see Fig. 1a and Supplementary Movie). For superficial injections, a local group of glomeruli was reliably targeted, selectively infecting almost 90% of all Cre positive interneurons locally (89 ± 3.7 %, n=8 slices, Supplementary Fig. 2a,b).

Thus, by taking advantage of the geometry of the OB and directed virus injections into deep and superficial layers we can selectively and efficiently manipulate GC and glomerular layer inhibition, respectively (Fig. 2a,b).

Theta phase segregation is mediated by glomerular layer circuits

To assess whether GC or glomerular layers set theta phases of OB principal neurons, we made whole-cell recordings from M/TCs *in vivo* combined with GCL or glomerular layer silencing in the anaesthetized preparation (Fig.2). Surprisingly, despite suppressing activity in >85% of all GCs, no depolarization or increase in M/TC firing occurred (mean baseline firing rate = 3.8 ± 0.5 Hz control vs 2.8 ± 0.4 Hz GCL silencing, p = 0.997 paired one-tailed t-test; Vm change = −1.0 ± 0.3 mV, p = 0.997, one-tailed t-test; n = 18 cells). Furthermore, slow rhythms in MCs and TCs were unaffected with preferred phases unaltered (Fig. 2c,e; p = 0.07, Fisher's rank test on circular distributions).

Silencing the glomerular layer on the other hand resulted in a small and variable firing rate change (median firing rate change = −0.7 Hz, 25th & 75th percentiles = [−2.0 −0.2] Hz; resting Vm = −48.0 ± 1.1 mV control vs −51.8 ± 1.08 mV LED; n = 23 cells). Notably sniff locking was drastically altered, including widespread phase shifts (ranging from −2.68 to 1.25 radians, p = 0.004, Fisher's rank test, n = 23 cells; Fig. 2d,f). This phase shift occurred particularly in cells that – in the absence of external stimuli - depolarize later in the sniff cycle. These neurons correspond to MCs (Fig. 2g; cf. ref [16]), suggesting that the baseline theta rhythm in the OB is structured by the local, glomerular inhibitory circuitry rather than from global, granule-cell mediated inhibition.

Feedforward inhibition in the glomerulus shapes theta rhythms

Glomerular circuits are highly intricate, where local interneurons collectively referred to as juxtaglomerular cells (JGCs) comprise several types partaking in a variety of feedforward, recurrent and local lateral inhibition[31,32]. In particular, inhibitory JGCs receiving direct olfactory nerve (ON) inputs, often referred to as ON-driven periglomerular cells or PGo cells, have been linked to the feedforward pathway[33]. Computational models postulated that such feedforward circuits likely inhibit MCs strongly, setting phase shift between MCs and TCs[16]. Understanding how such a circuit regulates theta range activity therefore required distinguishing these neurons *in vivo*. We achieved this by silencing projection neurons while recording from JGCs (Fig 3a), allowing JGCs that are predominantly driven by OB projection neurons to be distinguished from those driven predominantly by other sources, possibly ON. To this end we injected AAV for conditional expression of the light-gated cation channel ChR2 into the granule cell layer of Gad2-Cre mice (Fig 3a). Light presentation *in vivo* resulted in rapid and strong depolarization of, and action potential discharges in GCs (Fig. 3b), which in turn consistently and strongly hyperpolarized MCs and TCs (9/9 cells show 100% AP suppression; Fig. 3c,d). Whole-cell recordings from JGCs showed that spontaneous activity in some JGCs was drastically reduced as a consequence (Fig. 3e). Other JGCs showed no detectable alteration to spontaneous activity upon silencing M/TCs, demonstrating the dominant source of their excitatory drive to be other than OB projection neurons (Fig. 3f). We thus identified the latter population as putative "PGo" cells (Fig. 3g). PGos were physiologically more homogeneous judged by their respiration coupling: they preferably depolarized within a narrow range of respiratory phase (mean preferred Vm phase = 1.79 radians; 25-75 percentiles = [1.45 2.08] radians; n = 6 cells, Fig. 3h-k)), slightly preceding the trough of the MC theta rhythm (Fig. 3k), consistent with a role of PGo activity underlying hyperpolarization in MCs. JGCs in the residual population on the

other hand (JGr) were individually tuned to respiration albeit to vastly heterogeneous phases (Fig. 3l-o).

Thus, direct recordings demonstrate that putative PGo cells in the feedforward pathway in glomeruli likely mediate the phase shift between MC and TC theta rhythms.

Glomerular layer interneurons mediate slow inhibition

OB activity undergoes drastic changes in response to odors on both slow and fast timescales[11-13,34]. On slow timescales, odors frequently cause suppression of baseline firing in the principal neurons[13,19,20,34]. Such pauses in action potentials are thought to underlie at least one form of contrast enhancement of olfactory representations and are generally thought to originate from the lateral inhibition mediated by GCs[19-21]. To assess the synaptic basis of such pauses we presented a panel of odorants to anesthetized mice and measured the subthreshold activity in MCs and TCs. Consistent with earlier reports using extracellular recordings[13], sniff-locked inhibition (Fig. 4a) accounted for approximately one fifth of all responses (Fig. 4b).

To distinguish whether the evoked, sniff-coupled inhibition is mediated by the deep GC layer circuits or superficial glomerular circuits (Fig. 4c), we again employed layer-selective silencing of interneurons (Fig. 4d,e). Remarkably, with GC silencing, the evoked, sniff-locked inhibition was not reduced at all (evoked V_m = −2.6 ± 0.4 mV control vs. −3.1 ± 0.3 mV LED; n = 19 cells; Fig. 4d). In contrast, glomerular layer silencing consistently led to a significant reduction of evoked inhibition (evoked Vm −3.6 ± 0.6 mV control vs. −2.0 ± 0.4 mV LED; $p < 0.005$, n = 7 cells; Fig. 4e; Supplementary Fig. 3c), indicating that it is glomerular layer interneurons that underlie evoked, sniff-coupled inhibition.

Glomerular feed-forward circuits underlie slow inhibition

Some computational studies suggest that feed-forward inhibition in the glomerulus is an alternative explanation for inhibition evoked by odors[22]. In this case, PGo activity should coincide with evoked inhibition in M/TCs. Indeed, PGo cells identified as above (Fig. 3a-g) increase firing rates markedly in response to some odors, and such odor-evoked APs occur at times matching evoked inhibition in MCs and TCs (Supplementary Fig. 4a-d). Furthermore, increasing input strength by applying odors at increasing concentrations frequently converted inhibitory responses to excitatory responses (Supplementary Fig. 4e). This is again consistent with the involvement of parallel feedforward inhibition and excitation (see Supplementary Fig. 4i), where inhibition to the projection neuron dominates at lower input strengths, potentially due to the higher input resistance of PGos (see also ref[22]). This predicts that a total block of inhibition should unveil excitation at the input strength where inhibition normally dominates. To pharmacologically block inhibition *in vivo*, we applied a combination of $GABA_A$ antagonist gabazine and agonist muscimol, which blocks phasic synaptic inhibition while leaving basic network properties intact ("$GABA_A$-clamp", ref[16]). $GABA_A$-clamp not only completely abolished evoked, sniff-coupled inhibition but actually converted responses to phasic depolarization (−3.4 ± 0.7 mV control vs. 1.7 ± 0.4 mV $GABA_A$-clamp; $p < 0.01$, n = 11 cells; Fig. 5a, Supplementary Figure 4f). In many cases, this was accompanied by action potential discharge

(Supplementary Fig. 4h). This conversion to excitation occurred for the majority of evoked sniff-coupled inhibition but not for odors without detectable response during the control period (−0.2 ± 0.2mV control vs. −0.2 ± 0.1 mV $GABA_A$-clamp; range = [−0.80 0.90] mV control, [−0.66 0.04] mV $GABA_A$-clamp; p = 0.94, n = 7 cells; Fig. 5b, Supplementary Fig. 4f) again consistent with feedforward inhibition as a mechanism underlying slow odor-evoked inhibitory responses.

Thus, in contrast to common belief[19-21], it is the glomerular circuitry, likely via a feedforward inhibitory pathway, rather than the lateral inhibition by GCs, that underlies evoked inhibition on slow timescales and potentially contrast enhancement[22].

Granule cells co-ordinate fast activities

These results suggest that there is much weaker contribution from GCs on slow time scales than expected. The OB, however, is long renowned for the prominence of gamma range activity in addition to the slow rhythms[11]. Such activity is readily evoked by odor presentation in anaesthetized, as well as in awake, behaving animals[10] and has been hypothesized to emerge from synchronized synaptic interactions between GCs and the OB principal neurons[4,24,27]. Indeed, when silencing the GC layer, we found that individual, fast IPSPs in MCs were significantly suppressed *in vitro* (median change in IPSP frequency = −14.5 %; 25 and 75 percentiles = −42.1% and 2.8%; n = 25 cells; Supplementary Fig. 5). To probe the GC contribution to fast rhythms *in vivo*, we recorded the local field potential (LFP) from the GC layer in anesthetized animals. In line with previous studies, odor presentations caused a marked increase in power at gamma frequencies (Fig. 6a,b). As postulated based on previous pharmacological and modeling studies[4,24], GC silencing led to a significant reduction in this evoked power at gamma frequencies (evoked gamma power normalized to baseline = 1.8 ± 0.3 control vs. 1.3 ± 0.2 LED; p =0.002; n = 10 animals; Fig. 6a-c). Corresponding theta oscillations were again not affected (Fig. 6a). Silencing the glomerular circuitry on the other hand did not affect odor-evoked gamma (evoked gamma power normalized to baseline = 1.5 ± 0.1 control vs. 1.4 ± 0.1 LED; p = 0.48; n = 6 recordings from 4 animals).

We further investigated fast activities on a single cell level. Odors often evoke burst discharges of APs, during which pronounced regularity in the gamma frequency range is observed (Fig. 6d). Again, consistent with a key role of GCs in coordinating fast temporal features, the spike precision, specifically the regularity of spiking at fast gamma frequencies (65-100 Hz), was significantly reduced during GC silencing (mean spectral density estimates in the spike correlogram at high gamma = (0.2 ± 0.08) $*10^{-6}$ / Hz control vs. (0.08 ± 0.02) $*10^{-6}$ / Hz, LED; p = 0.02, n = 9 cells; Fig. 6d-f), without obvious changes in the firing rate (42.5 ± 4.0 Hz, control vs. 43.8 ± 13 Hz LED; p = 0.68, paired t-test, n = 9 cells; Supplementary Fig. 6).

Control of gamma and theta activity in the awake animal

Thus, GCs seem to coordinate high-frequency gamma activity in the OB, but contribute surprisingly little to slower, theta rhythms or sniff-coupled inhibition evoked by odors. While the anaesthetized preparation offers stability and thus permits more extensive

mechanistic investigations, there is accumulating evidence that neurons in the anesthetized and awake states may have different baseline excitability and/or firing rate[35-37]. This raises the possibility that GCs have a more prominent role in shaping slow activity in the awake preparation. To probe this, we performed whole-cell recordings from GCs and MCs *in vivo*, this time in the awake, head-fixed preparation. GCs in the awake preparation fired at similarly low rates compared to the anaesthetized cases (0.9 ± 0.0.3 Hz, n = 23 cells, compared to 0.6 ± 0.3 Hz in the anaesthetized, n = 43 cells). To assess the GC contribution to OB dynamics, we applied optogenetic GC silencing also in awake animals. In animals expressing ArchT in the GCL (AAV-FLEX-ArchT in Vgat-Cre animals as above), blind whole-cell patch clamp recordings from GCs revealed 13/15 cells (87%) hyperpolarized by more than 10 mV (Fig. 1f), indicating high infection rate and efficient silencing in the awake preparation as well. Such cells hyperpolarized by −22.0 ± 2.0 mV at depths ranging from −962 μm to −499 μm from the brain surface (Supplementary Fig. 2). Light-evoked hyperpolarization was strong enough to suppress odor-evoked excitatory responses in awake animals as well (Fig. 7a). To probe the contribution of GCs to fast network activity, we again recorded local field potentials while silencing the GC layer. Baseline LFP recordings in awake animals showed significantly more prominent gamma rhythms compared to the anesthetized state, consistent with recent reports[25]. Silencing GCs drastically reduced such gamma oscillations (Raw γ power = 135.6 ± 19.3 μV^2.s vs 108.5 ± 14.4 μV^2.s; $p < 0.01$, n = 11 recordings; Fig. 7b,c) confirming the key role of GCs in gamma activity in the awake. To analyze how GCs contribute to MC activity we performed whole-cell recordings from MCs in the awake state (Fig. 7d,e). Again, firing rates were largely unaltered by silencing GCs (3.94 ± 0.96 Hz control vs 3.21 ± 1.04 Hz LED; p = 0.43, n = 12 cells; Fig. 7d). Moreover, odor-evoked slow inhibitory responses, also observed prominently in the awake (8/16 odor-cell pairs, with an average hyperpolarization of −1.19 ± 0.43 mV), were not suppressed with GCL silencing (−2.55 ± 0.81 mV during LED; p = 0.90, one-tailed paired t-test; Fig. 7e).

Thus, as in the anesthetized preparation, GCs in the awake, too, underlie fast gamma rhythms, while not contributing to slow, respiration coupled odor-evoked inhibition.

Discussion

Altogether, our findings provide a mechanistic understanding of how inhibitory circuits within a brain region could shape signals in distinct ways. We demonstrate that inhibition from the local glomerular circuits sculpts slow rhythms by setting baseline phase as well as inhibiting OB output during odor presentations. Deep, global inhibitory circuits in the GC layer on the other hand refine temporal coherence in the gamma range and spike precision during odor presentation. This suggests dissociation between “slow” and “fast” inhibition in the olfactory bulb (Supplementary Fig. 1e), reminiscent of the pharmacological separation of slow and fast inhibition in insects[23].

Efficiency and extent of interneuron silencing

The lack of GC contribution to slow rhythms and sniff-coupled odor-evoked inhibition is particularly surprising. Immunohistochemistry and electrophysiological recordings show that virtually all GAD2 or VGAT positive granule cells were infected *in vivo* and *in vitro*

and hyperpolarized efficiently (Fig. 1; Supplementary Movie). Notably, *in vivo*, odor-evoked excitatory responses in GCs were reliably abolished. Therefore it is unlikely that the negative result can be attributed to omission of a significant subpopulation of GCs from our experimental manipulation. Lack of visible, slow depolarization in M/TCs upon GC silencing may relate to the low firing rates of GCs at rest *in vivo* we observe. While it is conceivable that local GABA release from the GC dendrites[38] might be affected less drastically, the widespread ArchT expression, including in the dendrites (Fig. 1), suppression of activities attributed to dendrodendritic inhibition, such as fast, recurrent IPSPs evoked in slices (Supplementary Fig. 5), and diminished gamma population responses *in vivo* (Figs. 6,7), make it unlikely that subthreshold dendritic release was completely unaffected by the optogenetic silencing of the GC layer. Rather, the absence of *any* phase shift of slow rhythms or suppression of odor-evoked inhibition during GC layer silencing strongly suggests that GCs do not play a role in coordinating these slow activities. Furthermore, optogenetic silencing of only a local group of glomerular interneurons was sufficient to reduce phase-shift in MCs and reduce evoked inhibition drastically (Figs. 2, 4). The fact that glomerular silencing did not convert evoked inhibition into excitation as reliably as the pharmacological manipulation (Fig. 5) might indicate that, even though M/TCs recorded were in the immediate vicinity of injection sites, they did not always extend their apical dendritic tufts into the core of the infected region where infection only incompletely covers the JGC population (Supplementary Fig. 3a). While incomplete silencing would be potentially problematic for negative results, it is difficult to deny the glomerular layer contribution to slow inhibition from the strong effects observed during glomerular silencing. It is likely that our layer-selective silencing included some interneurons outside glomerular and GC layers, such as EPL interneurons. While they are likely to contribute importantly to OB function[39,40], their broad odor tuning may preclude inhibition of M/TC activity matched to excitation described here.

Mechanisms underlying gamma-band activity

A number of studies based on models[4], current source density analysis[10], localized pharmacology[24] and constitutive genetic modifications[25,27] suggest that the dendrodendritic MC-GC synapse might underlie gamma activity. Our results from optogenetic silencing of the GC layer provide direct evidence of a causal role for GCs in gamma oscillations in anesthetized and awake animals. The remaining gamma power during GC silencing may be explained by the autonomous dendritic mechanisms for GABA release not involving somatic APs[38] mentioned earlier or the residual 10-15% of GCs might have escaped the manipulation. Alternatively, the condition could have additionally silenced other interneuron types present in the GC layer, such as Blanes cells that inhibit GCs tonically[41,42], possibly amplifying remaining GC contributions.

We have discussed until now gamma oscillations largely as one band. However, this band in the OB consists of at least two types, namely slow and fast gamma oscillations[10], thought to involve MCs and TCs, respectively[43]. We have analyzed the standard broad gamma band (40-100 Hz)[10] in the LFP, and only at single cell level managed to highlight fast gamma range activity as spike regularity in TCs thought to arise from their higher firing rates[43]. In

both cases, gamma activities strongly relied on GCs - consistent with a dominant role of the GCL in coordinating synchrony on fast timescale.

Temporal separation by glomerular feed-forward inhibition

Rhythmic, sniff coupled patterning of activity has attracted attention for more than 60 years[11] and has been intensely studied especially in the anesthetized preparation. Both principal neurons and interneurons demonstrate a prominent subthreshold oscillation[14,16,18]. However because the difference in respiration coupling of mitral and tufted cells was reported only recently, mechanistic understanding here is much scarcer. Rhythmicity in GC activation and the consequent rhythmic inhibition of M/TC lateral inhibition have long been linked to the sniff coupling patterns of M/TCs[14,17,18], but recent computational models suggested the glomerular feedforward circuitry as a possible mechanism behind the MC-TC phase shift[16]. Our experiments here showed that silencing GCs has negligible effect on baseline activity of MCs and TCs including depth of modulation or preferred phase of discharge. Instead, drastic alteration in sniff coupling was observed with glomerular layer silencing. The largest phase shift occurred in cells identified as MCs based on their subthreshold oscillations, consistent with the earlier report that temporal separation is established by delaying MCs by inhibition[16]. Here we further attempted to dissect the intricate glomerular circuit. As there is no specific molecular marker for neurons involved in the feedfoward pathway[32], we relied on functional connectivity to distinguish JGC classes : by shutting down activity in MCs and TCs via optogenetic activation of GCL interneurons, we could identify JGCs based on the source of excitatory drive. This would include cells exclusively driven by the ON and may also comprise other cell types such as those driven by glomerular feed-forward excitation described *in vitro*[32]. Most recorded JGCs locked tightly to respiration rhythms as reported recently[44], but with a variety of phase preferences. The putative PGo population functionally distinguished was more homogenous, depolarising within a narrow phase window that corresponded to the MC hyperpolarization. This method for circuit analysis *in vivo* relied on the neatly layered structure of the OB but might prove to be useful in other brain areas as well.

All together, our data excludes GCs as a major source of respiration-linked hyperpolarization in MCs but strongly suggests PGo-mediated feedforward inhibition as the mechanism underlying the phase delay of MCs. This delay might be used for readout of OB activity in the piriform cortex[14] and might additionally give MCs the necessary temporal window to integrate information computed across the OB. Such “across-channel” computation could involve recruitment of GCs as shown to be implicated for tasks that are known to take more time[45,46].

Odor-evoked inhibition and contrast enhancement

Contrast enhancement is a widespread feature of sensory representation in general and is thought to be one of the central roles for lateral inhibition in the brain. Inhibitory responses prominently observed in M/TCs in anesthetized animals have for decades been linked to this idea, fuelled by the observation that some odorants, which are structurally similar to odorants that excite a recorded M/TC, can inhibit them[20], reminiscent of a “centre-surround” arrangement[20,21]. Although such evoked inhibition has frequently been referred to as

"lateral inhibition", direct evidence for an involvement of GCs has been missing. Here we show that surprisingly silencing of GCs did not affect slow, odor-evoked inhibition. It was rather glomerular silencing that reliably suppressed this inhibition. Furthermore, our pharmacological manipulation revealed evoked excitation that is normally masked by evoked inhibition - an effect never seen for odors without detectable responses under control conditions (Fig. 5). Such strict concurrence between evoked inhibition and excitation is difficult to reconcile with the GC "lateral inhibitory" network as an underlying mechanism, as there is no canonical accompanying source of excitation (Fig. 4c; Supplementary Fig. 4). Rather, it is indicative of parallel feed-forward excitation / inhibition pathways, which are present mainly in the glomerular layer (Figs. 3,4c; ref[32,33]). Consistent with this, PGo neurons discharge at times matching evoked inhibition making them a possible candidate for this phenomenon. Whether the population of PGo cells underlying the phase shift between MCs and TCs is identical, overlapping or distinct from the population of PGo mediating odor-evoked inhibition remains to be determined.

It is tempting to speculate that what we described here is an implementation of "non-topographical contrast enhancement (NTCE[22])". In this model olfactory representation is sharpened "within-channel" as follows: a glomerulus only weakly tuned to a given odor receives excitation not strong enough to activate M/TCs but able to recruit more electrotonically compact PG cells via a feedforward pathway, resulting in inhibition of OB outputs. This is an attractive alternative, as olfactory stimuli lack a simple spatial relationship that is evident in visual stimuli[22]. Here we demonstrate experimentally glomerular circuits, particularly the feedforward pathway, as the possible source of slow inhibition associated with contrast enhancement and exclude a role for GCs in this.

Conclusion

The scenario that emerges is one where the glomerular circuit gives primary structure to olfactory inputs locally, producing diversity between mitral and tufted cells and possibly enhancing contrast non-topographically in neurons associated with one glomerular "channel". The deeper granule layer in turn further refines signals by orchestrating activity over the OB using precise timing, which is likely critical for efficient integration in downstream cortical structures[47].

The general idea of dissociable rate and temporal codes has been explored e.g. in the hippocampus where firing rate and phase within a theta cycle have been suggested to represent different variables[48]. In addition, APs within each theta cycle can be organized even more precisely through gamma rhythms nested within the theta rhythm[9]. Alternatively, multiple signals might coexist as a mechanism to minimize signal corruption by multiplexing signals across several frequency bands[49]. Recruitment of distinct circuits within a brain region for dissociable control of activities on such different timescales is likely to prove important in all these cases.

Online METHODS

All animal experiments were performed according to the guidelines of the German animal welfare law, approved by the local ethics panel and UK Home Office under the Animals (Scientific Procedures) Act 1986. Mice used for the optogenetic experiments were from transgenic lines expressing Cre-recombinase in GAD2-expressing or VGAT-expressing neurons (Gad2-ires-Cre or VGat-ires-Cre; from Jackson laboratories and Bradford Lowell, Harvard). Both male and female mice were used. All reagents were obtained from Sigma Aldrich unless noted otherwise.

Virus generation and stereotactic injections

AAV-EF1A-DIO-Chr2-GFP (ref[50]) and AAV-CAG-FLEX-ArchT-GFP (ref[28]) were produced using a protocol described elsewhere[51] to titers of $1.3*10^{13}$ particles/ml and $6.1*10^{12}$ particles/ml, respectively.

Animals were anaesthetized intraperitoneally with ketamine and xylazine (100 mg/kg and 20 mg/kg, respectively) and prepared for surgery in a stereotactic frame (David Kopf Instruments, Tujunga CA, USA). For injection of AAV, five co-ordinates were used for targeting the GC layer, where virus was dispensed at 3 and 2 depths along the first and second tracks. The co-ordinates were: for the first track: +0.75 mm (anteroposterior, AP), −0.75 mm (mediolateral, ML) from the midline rhinal fissure, at three dorsoventral (DV) depths, −0.7 mm (207 nl), −1.1 mm (103.5 nl) & −1.3 mm (103.5 nl); for the second track: +1.1 mm (AP), −0.75 mm (ML) from the midline rhinal fissure, at two depths, −0.7 mm (207 nl dispensed), −1.15 mm (103.5 nl). For targeting the glomerular layer, the co-ordinate was +2.0 mm (AP), −1.0 mm (ML), −0.3 mm (DV), with 92 nl injected at a single site. This coordinate was chosen to target dorsolaterally located glomeruli, ideal for subsequently targeting MCs belonging to those glomeruli. Furthermore, for glomerular layer injections the head of the animals were tilted leftwards and backwards by 15 degrees and 10 degrees, respectively, so that the craniotomy for virus injection was as far away as possible from the craniotomy for electrophysiological recordings. Such injections resulted in approximately 95% of all infected cells being located in the GL (Supplementary Fig. 3). Viruses were dispensed from a thin capillary tube using a Nanoject injector (Drummond Scientific, Broomall, PA, USA) at a rate of 46 nl per minute. Animals were 28-45 days old at the time of injections. Electrophysiology was carried out 1-4 weeks after the virus injections.

In vivo *Electrophysiology*

Animals were anesthetized intraperitoneally with ketamine and xylazine (100 mg/kg and 20 mg/kg, respectively for induction; xylazine concentration was reduced to 10 mg/kg for maintenance) and kept warm (37°C; DC temperature controller, FHC, Bowdoin ME, USA) for the duration of the experiments. A small craniotomy and durectomy of approximately 500 μm in diameter was made over the dorsolateral part of the left olfactory bulb, which was submerged in Ringer solution containing (in mM): NaCl (135), KCl (5.4), HEPES (5), MgCl2 (1), CaCl2 (1.8), and its pH adjusted to 7.2 and 280 mOsm/kg. Whole-cell recordings were made with borosilicate glass pipette filled with (in mM): KMeSO4 (130), HEPES (10), KCl (7), ATP_2-Na (2), ATP-Mg (2), GTP (0.5), EGTA (0.05), biocytin (10),

with pH and osmolarity adjusted to 7.3 and 275-80 mOsm/kg, respectively. Signals were amplified and filtered at 30 kHz by an Axoclamp 2B (Molecular Devices, Sunnyvale, CA, USA) and digitized at 20 kHz with a micro 1401 (Cambridge Electronic Design, Cambridge, UK). Neurons were identified based on depth and passive membrane properties, and in some cases confirmed with morphology (ref 16; Fig 1g). PGo cells were functionally distinguished from JGr cells by assessing the major source of excitatory drive (Fig. 3). Depths of recorded neurons are vertical distances from the brain surface. Respiration was recorded using a piezoelectric band (Kent Scientific, Torrington, CT, USA) wrapped around the animal's chest and calibrated against nasal flow as previously described[16]. For morphological identification of some recorded neurons, recorded OBs were sectioned and stained for biocytin using an avidinbiocytin reaction coupled to peroxidase/DAB reaction[52] (ABC kit, Vector Labs, Peterborough, UK). Stained cells were traced using a Neurolucida system (MBF Bioscience, Williston, VT, USA).

Recordings from awake animals were performed as described previously[16]. In brief, 30-50 day old C57BL/6 mice or Vgat-Cre mice previously injected with AAV were implanted with a stainless steel head-plate and allowed to recover. On the day of the experiments, animals were given meloxicam (2.5 mg/kg, s.c.) or carprofen (5 mg/kg, s.c.) and lidocaine (1%, s.c.) or levobupivacaine (0.5 %, s.c.) pre-operatively. Under isoflurane anesthesia (1.75% in air), a craniotomy approximately 2 mm in diameter was made over the dorsal surface of the olfactory bulb, which was subsequently covered with a thin layer of agarose (5% in the Ringer solution) for stability. The animals were allowed to recover from the isoflurane anesthesia for at least 30 minutes before recordings commenced. After this time such head-fixed animals readily perform olfactory discrimination tasks during whole cell recordings (M.K., A. Schmaltz, I.F., A.T.S., Soc. Neurosci. Abstr. 2012).

Illumination for the optogenetic experiments *in vivo* in both anesthetized and awake preparations was presented by an XP-G LED (Cree, Durham NC, USA) placed approximately 1 cm above the brain surface so that it produced ~15 mW/mm^2 of light intensity on the surface. For experiments with odor presentations, control trials and trials with LED were interleaved for all experiments. For effects on spontaneous activity, light was presented for 1 second every 10 seconds.

$GABA_A$-clamp was carried out in a manner previously described[16]. Briefly, a solution containing gabazine and muscimol (0.45 mM and 2 mM, respectively; Tocris Biosciences, Bristol, UK) was superfused over the exposed brain using a peristaltic pump (Ismatec, IDEX Health & Science, Wertheim-Mondfield, Germany). The solution was superfused for at least 30 minutes for the drug condition. Odors at concentrations of 0.1-10% of saturated vapor (up to 35% in Supplementary Fig. 4e) were presented at 30-second intervals using a custom-made olfactometer timed to the peak of expiration detected from the chest distension signals (Spike-Height discriminator, FHC, Bowdoin ME, USA). A panel of odorants presented consisted of isoamylacetate, methylsalicylate, salicylaldehyde, cinnamaldehyde, eugenol, acetophenone, cineol, and mineral oil (analytical standard). When all 7 odors were presented, 47% of cells responded with excitation to at least one odor. Inhibition in response to at least one odor was observed in 16% of all cells.

In vitro *electrophysiology*

Dissected OBs were submerged in ice-cold artificial cerebrospinal fluid (ACSF) containing (in mM): NaCl (125), $NaHCO_3$ (25), NaH_2PO_4 (1.25), glucose (25), KCl (2.5), $MgCl_2$ (2) and $CaCl_2$ (1), equilibrated with a mixture of 95 % O_2 and 5% CO_2 and adjusted to 310 - 320 mOsm osmolarity, and horizontal slices 300 μm in thickness were made using a vibratome (Microm HM650V, Sigmann Elektronik, Hüffenhardt, Germany). For electrophysiology, the concentration of $MgCl_2$ and $CaCl_2$ were changed to 1 mM and 2 mM, respectively, and the solution was warmed to 33-35 °C. Whole-cell recordings were made with borosilicate glass electrodes filled with the same internal solution used for *in vivo* electrophysiology, except the exclusion of biocytin. Signals were amplified by a Multiclamp 700B (Molecular Devices, Sunnyvale, CA, USA), digitized at 16.67 kHz by an ITC 16 (HEKA, Lambrecht/Pfalz, Germany) and acquired using the NClamp/Neuromatic package (Jason Rothman, http://www.thinkrandom.com) in Igor Pro (Wavemetrics, Lake Oswego, OR, USA). The halogen microscope light source (100W; Zeiss, Jena, Germany) was used for optogenetic experiments *in vitro*.

Data Analysis

Data was analyzed in Spike2 (CED, Cambridge, UK), Matlab (Mathworks, Natick Massachusetts, USA) and Igor Pro using custom-written routines. Unless otherwise stated, values stated in the text are the mean and the standard error of the mean. Sample sizes used are similar to those reported in the field and no statistical method was used to predetermine these. p-values reported are, unless otherwise stated, from 2-tailed paired t-tests. For statistical tests requiring normal underlying distributions, normality was assumed while individual data points are displayed wherever possible. Data collection and analysis were not performed blind to the conditions of the experiments. One sniff cycle is defined to be from one expiration peak to the next expiration peak. Expiration peaks were the most reliable events for detection. On average, expiration peak occurs approximately 100 ms after the inhalation onset in anaesthetized mice[16]. Recordings were aligned and normalized to the sniff cycle and significance of sniff coupling was assessed as described previously[16]. *Vm change with light for testing the optogenetic method:* average Vm during baseline period (a 500 ms window approximately 100 ms before light onset) was subtracted from average Vm during light (a 500 ms window approximately 150 ms after light onset). *Light-induced phase shift*: preferred phase of sniff aligned, subthreshold membrane potential average was obtained as described previously[16] and compared to the baseline periods (5 s before the light onset) and during light (all complete sniff cycles during light presentations). Light presentation was for 1 s. This was repeated for at least 20 times every 10 seconds. Preferred phase was calculated as the phase of an average vector, where sniff phase and the baseline-subtracted Vm amplitude corresponded to the argument and magnitude of individual vectors. Phase-shift was the preferred phase during light minus the preferred phase during baseline, and is given in radians. *Fisher's rank test on two circular distributions*: non-parametric tests comparing two circular histograms were carried out as described in Fisher[53] (page 122). Comparison was between the distribution of phaseshifts during silencing and the distribution of baseline phase fluctuations (φbaseline2-φbaseline1, φbaseline1 = preferred phase during 5 seconds before each LED presentation, φbaseline2 = preferred phase

between 6 seconds and 5 seconds before LED presentation). Phaseshifts and baseline phase fluctuations were circularly ranked together[53] and the resulting rank vectors compared against test statistics from randomly generated ranks (1000 sets) to obtain the p values. *Drift subtraction*: During light presentations, a small drift of baseline membrane potential (−0.82 ± 0.71 mV /cycle) was observed, which was subtracted for display purpose only (Fig 2d). *Color-coding of MC/TC likelihood*: The [R G B] values were determined as [1–0.9*Vm_{TC} (φ), 1–0.9*Vm_{MC}–0.5*Vm_{TC} (φ), 1–0.3*Vm_{MC} (φ)], where Vm_{TC}(φ) and VM_{MC}(φ) correspond to the sniff-aligned average subthreshold membrane potential from identified TCs and MCs (measured in ref[16]), respectively, at the corresponding phase. This resulted in cells that lock to the average MC phase to appear bright pink, cells locking to the average TC phase cyan and cells at the border between MC and TC phase region to be plotted in pale colors[16]. *Detection of odor responses (Fig. 4)*: Baseline Vm fluctuation was subtracted sniff-by-sniff[46]. A deviation greater than 2 standard deviations of the baseline fluctuation during the first three sniff cycles after the valve opening was termed a response. A significantly negative deviation not accompanied by AP increase was classified as a purely hyperpolarizing response ("slow inhibition"). AP change was defined as an increase in the number of APs per sniff of more than 2 standard deviations above the baseline fluctuation. Excitatory response was defined as a positive AP change during the first 3 sniff cycles after the valve opening. *Vm changes evoked by odor presentations (Evoked Vm):* Evoked Vm was obtained by subtracting the average baseline Vm (Vm during 5 s before odor onset) from average Vm during odor application (for 1s since valve opening). Baseline drift due to light presentation alone was subtracted (−6.26 ± 1.29 mV for glomerular layer silencing, n = 7 cells; no drift subtraction was necessary for GCL silencing – see Results). For illustration capacitive artefacts from LED/Valve activation were removed in some figures. *Spectral analysis*: Estimates of spectral densities were obtained using a multi-taper method (http://chronux.org; ref[54]), with time window 0.5 s (T*W = 2, and 3 tapers used[55]). Density estimates from evoked period (1 s since odor onset) were divided by those from baseline period (1 second before odor onset). *Spike precision during GC silencing*: spikes evoked in tufted cells during odor presentations (n = 10 cells) were analyzed. Display of spike regularity (Fig 6d,e) was achieved by realigning spike times with respect to each spike ($Spike_{ref}$; ref[56]). Correlograms of spikes were obtained for spikes within and across trials, which were averaged and spectral density estimates obtained for each cell by the multi-taper method (window = 0.5 s; T*W=5, 9 tapers used). *Baseline variability in firing rate*: the average firing rate during 1-second window before LED presentation ($FR_{Control1}$) and the average firing rate during another 1-second window starting 2 seconds before LED presentation ($FR_{Control2}$) were measured to obtain $FR_{Control2}$-$FR_{Control1}$ (baseline variability). The average baseline variability for all LED trials for each cell was averaged and summarized in the histogram (Fig. 7d). A supplementary methods checklist is available.

Supplementary Material

Refer to Web version on PubMed Central for supplementary material.

Europe PMC Funders Author Manuscripts

Acknowledgements

We thank Marlies Kaiser, Ellen Stier and Gwenaelle Matthies for technical assistance, Andreas Balz and Sabine Martin for stereotactic injections, Sebastiano Belanca for morphological reconstructions, Janine Reinert for virus characterization, Anja Schmaltz and Mostafa Abdelhamid for help with setting up the head-fixed awake preparation, Günter Giese and Annemarie Scherbarth for glass brain preparation and imaging, Bradford Lowell, Linh Vong, and Venkatesh Murthy for providing Vgat-ires-Cre knock-in mice, Rolf Sprengel for the cre-antibody, Troy Margrie, Thomas Cleland, and Winfried Denk for discussion and Troy Margrie, Denis Burdakov, Hannah Monyer, Rebecca Jordan, Agnieszka Grabska-Barwińska and Moritz Helmstaedter for comments on earlier versions of the manuscript. This work was supported by the MPG, the DFG-SPP1392, the BMBF (US-German collaboration computational neuroscience), AvH, MRC (MC_UP_1202/5), the ExcellenzCluster CellNetworks, and the Gottschalk foundation.

References

1. Wachowiak M. All in a Sniff: Olfaction as a Model for Active Sensing. Neuron. 2011; 71:962–973. [PubMed: 21943596]
2. Smear M, Shusterman R, O'Connor R, Bozza T, Rinberg D. Perception of sniff phase in mouse olfaction. Nature. 2011; 479:397–400. [PubMed: 21993623]
3. Haddad R, et al. Olfactory cortical neurons read out a relative time code in the olfactory bulb. Nat. Neurosci. 2013; 16:949–957. [PubMed: 23685720]
4. Freeman, WJ, III. Waves, Pulses, and the Theory of Neural Masses. Academic Press; 1972. 1972
5. Sohal VS, Zhang F, Yizhar O, Deisseroth K. Parvalbumin neurons and gamma rhythms enhance cortical circuit performance. Nature. 2009; 459:698–702. [PubMed: 19396159]
6. Royer S, et al. Control of timing, rate and bursts of hippocampal place cells by dendritic and somatic inhibition. Nat. Neurosci. 2012; 15:769–775. [PubMed: 22446878]
7. Klausberger T, Somogyi P. Neuronal Diversity and Temporal Dynamics: The Unity of Hippocampal Circuit Operations. Science. 2008; 321:53–57. [PubMed: 18599766]
8. Whittington MA, Traub RD. Interneuron Diversity series: Inhibitory interneurons and network oscillations in vitro. Trends Neurosci. 2003; 26:676–682. [PubMed: 14624852]
9. Lisman JE, Jensen O. The Theta-Gamma Neural Code. Neuron. 2013; 77:1002–1016. [PubMed: 23522038]
10. Kay LM, et al. Olfactory oscillations: the what, how and what for. Trends Neurosci. 2009; 32:207–214. [PubMed: 19243843]
11. Adrian ED. The electrical activity of the mammalian olfactory bulb. Electroencephalogr. Clin. Neurophysiol. 1950; 2:377–388.
12. Macrides F, Chorover SL. Olfactory Bulb Units: Activity Correlated with Inhalation Cycles and Odor Quality. Science. 1972; 175:84–87. [PubMed: 5008584]
13. Shusterman R, Smear MC, Koulakov AA, Rinberg D. Precise olfactory responses tile the sniff cycle. Nat. Neurosci. 2011; 14:1039–1044. [PubMed: 21765422]
14. Margrie TW, Schaefer AT. Theta oscillation coupled spike latencies yield computational vigour in a mammalian sensory system. The Journal of Physiology. 2003; 546:363–374. [PubMed: 12527724]
15. Igarashi KM, et al. Parallel Mitral and Tufted Cell Pathways Route Distinct Odor Information to Different Targets in the Olfactory Cortex. The Journal of Neuroscience. 2012; 32:7970–7985. [PubMed: 22674272]
16. Fukunaga I, Berning M, Kollo M, Schmaltz A, Schaefer AT. Two Distinct Channels of Olfactory Bulb Output. Neuron. 2012; 75:320–329. [PubMed: 22841316]
17. Phillips ME, Sachdev RNS, Willhite DC, Shepherd GM. Respiration Drives Network Activity and Modulates Synaptic and Circuit Processing of Lateral Inhibition in the Olfactory Bulb. The Journal of Neuroscience. 2012; 32:85–98. [PubMed: 22219272]
18. Cang J, Isaacson JS. In Vivo Whole-Cell Recording of Odor-Evoked Synaptic Transmission in the Rat Olfactory Bulb. The Journal of Neuroscience. 2003; 23:4108–4116. [PubMed: 12764098]
19. Luo M, Katz LC. Response Correlation Maps of Neurons in the Mammalian Olfactory Bulb. Neuron. 2001; 32:1165–1179.

20. Yokoi M, Mori K, Nakanishi S. Refinement of odor molecule tuning by dendrodendritic synaptic inhibition in the olfactory bulb. Proceedings of the National Academy of Sciences. 1995; 92:3371–3375.
21. Shepherd GM, Chen WR, Willhite D, Migliore M, Greer CA. The olfactory granule cell: From classical enigma to central role in olfactory processing. Brain Research Reviews. 2007; 55:373–382. [PubMed: 17434592]
22. Cleland TA, Sethupathy P. Non-topographical contrast enhancement in the olfactory bulb. BMC Neuroscience. 2006; 7:7. [PubMed: 16433921]
23. MacLeod K, Laurent G. Distinct Mechanisms for Synchronization and Temporal Patterning of Odor-Encoding Neural Assemblies. Science. 1996; 274:976–979. [PubMed: 8875938]
24. Lagier S, Carleton A, Lledo P-M. Interplay between Local GABAergic Interneurons and Relay Neurons Generates Gamma Oscillations in the Rat Olfactory Bulb. The Journal of Neuroscience. 2004; 24:4382–4392. [PubMed: 15128852]
25. Lepousez G, Lledo P-M. Odor Discrimination Requires Proper Olfactory Fast Oscillations in Awake Mice. Neuron. 2013; 80:1010–1024. [PubMed: 24139818]
26. Bathellier B, Lagier S, Faure P, Lledo P-M. Circuit Properties Generating Gamma Oscillations in a Network Model of the Olfactory Bulb. J. Neurophysiol. 2006; 95:2678–2691. [PubMed: 16381804]
27. Nusser Z, Kay LM, Laurent G, Homanics GE, Mody I. Disruption of GABAA Receptors on GABAergic Interneurons Leads to Increased Oscillatory Power in the Olfactory Bulb Network. J. Neurophysiol. 2001; 86:2823–2833.
28. Han X, et al. A high-light sensitivity optical neural silencer: development and application to optogenetic control of non-human primate cortex. Frontiers Systems Neurosci. 2011; 5
29. Taniguchi H, et al. A Resource of Cre Driver Lines for Genetic Targeting of GABAergic Neurons in Cerebral Cortex. Neuron. 2011; 71:995–1013. [PubMed: 21943598]
30. Vong L, et al. Leptin Action on GABAergic Neurons Prevents Obesity and Reduces Inhibitory Tone to POMC Neurons. Neuron. 2011; 71:142–154. [PubMed: 21745644]
31. Parrish-Aungst S, Shipley MT, Erdelyi F, Szabo G, Puche AC. Quantitative analysis of neuronal diversity in the mouse olfactory bulb. The Journal of Comparative Neurology. 2007; 501:825–836. [PubMed: 17311323]
32. Kiyokage E, et al. Molecular Identity of Periglomerular and Short Axon Cells. The Journal of Neuroscience. 2010; 30:1185–1196. [PubMed: 20089927]
33. Najac M, De Saint Jan D, Reguero L, Grandes P, Charpak S. Monosynaptic and Polysynaptic Feed-Forward Inputs to Mitral Cells from Olfactory Sensory Neurons. The Journal of Neuroscience. 2011; 31:8722–8729. [PubMed: 21677156]
34. Margrie TW, Sakmann B, Urban NN. Action potential propagation in mitral cell lateral dendrites is decremental and controls recurrent and lateral inhibition in the mammalian olfactory bulb. Proceedings of the National Academy of Sciences. 2001; 98:319–324.
35. Kato HK, Chu MW, Isaacson JS, Komiyama T. Dynamic Sensory Representations in the Olfactory Bulb: Modulation by Wakefulness and Experience. Neuron. 2012; 76:962–975. [PubMed: 23217744]
36. Rinberg D, Koulakov A, Gelperin A. Sparse Odor Coding in Awake Behaving Mice. The Journal of Neuroscience. 2006; 26:8857–8865. [PubMed: 16928875]
37. Cazakoff BN, Lau BYB, Crump KL, Demmer HS, Shea SD. Broadly tuned and respiration-independent inhibition in the olfactory bulb of awake mice. Nat. Neurosci. 2014; 17:569–576. [PubMed: 24584050]
38. Isaacson JS, Strowbridge BW. Olfactory Reciprocal Synapses: Dendritic Signaling in the CNS. Neuron. 1998; 20:749–761. [PubMed: 9581766]
39. Kato HK, Gillet SN, Peters AJ, Isaacson JS, Komiyama T. Parvalbumin-Expressing Interneurons Linearly Control Olfactory Bulb Output. Neuron. 2013; 80:1218–1231. [PubMed: 24239124]
40. Miyamichi K, et al. Dissecting Local Circuits: Parvalbumin Interneurons Underlie Broad Feedback Control of Olfactory Bulb Output. Neuron. 2013; 80:1232–1245. [PubMed: 24239125]
41. Labarrera C, London M, Angelo K. Tonic inhibition sets the state of excitability in olfactory bulb granule cells. The Journal of Physiology. 2013; 591:1841–1850. [PubMed: 23318869]

42. Pressler RT, Strowbridge BW. Blanes Cells Mediate Persistent Feedforward Inhibition onto Granule Cells in the Olfactory Bulb. Neuron. 2006; 49:889–904. [PubMed: 16543136]
43. Manabe H, Mori K. Sniff rhythm-paced fast and slow gamma-oscillations in the olfactory bulb: relation to tufted and mitral cells and behavioral states. J. Neurophysiol. 2013; 110:1593–1599. [PubMed: 23864376]
44. Livneh Y, Adam Y, Mizrahi A. Odor Processing by Adult-Born Neurons. Neuron. 2014
45. Shimshek DR, et al. Enhanced Odor Discrimination and Impaired Olfactory Memory by Spatially Controlled Switch of AMPA Receptors. PLoS Biol. 2005; 3:e354. [PubMed: 16216087]
46. Abraham NM, et al. Synaptic Inhibition in the Olfactory Bulb Accelerates Odor Discrimination in Mice. Neuron. 2010; 65:399–411. [PubMed: 20159452]
47. MacLeod K, Backer A, Laurent G. Who reads temporal information contained across synchronized and oscillatory spike trains? Nature. 1998; 395:693–698. [PubMed: 9790189]
48. Huxter J, Burgess N, O'Keefe J. Independent rate and temporal coding in hippocampal pyramidal cells. Nature. 2003; 425:828–832. [PubMed: 14574410]
49. Akam TE, Kullmann DM. Efficient ,"Communication through Coherence," Requires Oscillations Structured to Minimize Interference between Signals. PLoS Comput Biol. 2012; 8:e1002760. [PubMed: 23144603]
50. Tsai H-C, et al. Phasic Firing in Dopaminergic Neurons Is Sufficient for Behavioral Conditioning. Science. 2009; 324:1080–1084. [PubMed: 19389999]
51. During, M.; Young, D.; Baer, K.; Lawlor, P.; Klugmann, M. Viral Vectors for Gene Therapy. Machida, CurtisA, editor. Vol. Vol. 76 Methods in Molecular Medicine,Ñ¢. Humana Press; 2003. p. 221-236.Ch. 11
52. Marx M, Gunter RH, Hucko W, Radnikow G, Feldmeyer D. Improved biocytin labeling and neuronal 3D reconstruction. Nat Protoc. 2012; 7:394–407. [PubMed: 22301777]
53. Fisher, NI. Statistical Analysis of Circular Data. Cambridge University Press; 1996. 122 1996
54. Mitra, P.; Bokil, H. Observed Brain Dynamics. Oxford University Press; USA: 2007. 2007
55. Kay LM, Lazzara P. How Global Are Olfactory Bulb Oscillations? J. Neurophysiol. 2010; 104:1768–1773. [PubMed: 20660428]
56. Gabbiani, F.; Koch, C. Methods in neuronal modeling: from synapses to networks. Koch, Christof; Segev, Idan, editors. MIT Press; 1998. p. 313-360.

Europe PMC Funders Author Manuscripts

Europe PMC Funders Author Manuscripts

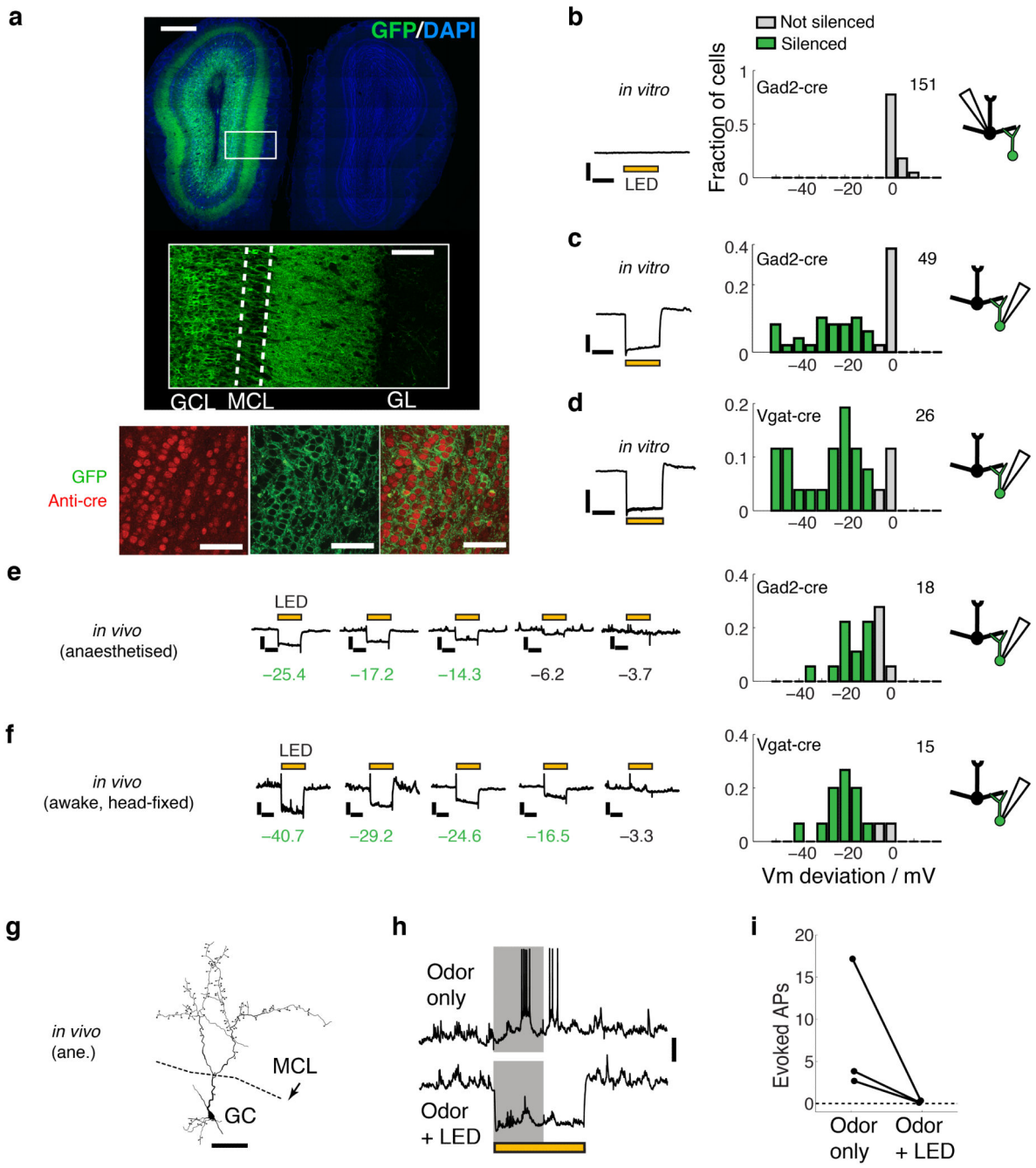

Figure 1. Efficiency and specificity of optogenetic silencing of granule cells

Assessment of specificity and effectiveness of infection in OB slices and *in vivo*. (**a**) Expression pattern in the OB following GCL injection in a Gad2-Cre animal (top). The region marked by the white box is shown zoomed in the inset. GCL, MCL and GL correspond to granule cell layer, mitral cell layer and glomerular layer. Scale bars for the overview and inset = 0.5 mm and 0.1 mm. See also the Supplementary Movie of a z-stack across the entire OB showing GFP expression pattern in the whole OB. Bottom: Immunohistochemical assessment of infection efficiency in a Vgat-Cre animal: top panel

shows cre-immunoreactivity in red, middle panel shows raw GFP fluorescence in green. Bottom panel is the overlay of red and green signals. Scale bar = 50 μm. Image section taken from the center of the GCL. (**b-f**) Electrophysiological assessment of infection and silencing efficiency and selectivity. (**b**) Example whole cell recordings from MCs in OB slices from Gad2-Cre animals injected with AAV-FLEX-ArchT in the GCL during light presentation (left; yellow bar indicates light presentation). Scale bars = 20 mV, 0.5 s. Summary histogram (right) shows proportion of recorded cells with corresponding light evoked Vm deviation. Vm deviation more negative than 10 mV is marked green ("silenced"). The number on the top right corner is the total number of cells recorded. (**c,d**) as in (**b**) but recordings were from randomly selected GCs from GCL-injected Gad2-Cre (**c**) or Vgat-Cre (**d**) animals. Scale bars = 20 mV, 0.5 s. (**e,f**) *in vivo* assessment of GC silencing in Gad2-Cre, anesthetized animals (**e**) and Vgat-Cre, awake, head fixed animals (**f**). Data were from 5 and 3 animals, respectively. Traces in the middle are examples from different cells and numbers below indicate measured Vm deviation with the same colour coding as the histograms. Scale bars = 20 mV, 0.5 s. (**g-i**) GC silencing during excitatory odor responses *in vivo.* (**g**) Example of a reconstructed GC morphology. (**h**) Action potentials evoked by 1s odor presentation (gray) under control condition (top trace). Response to the same odorant during light presentation (bottom trace). Scale bar = 10 mV. (**i**) Summary data showing average number of APs evoked during 1s odor presentation, for odor only and with additional light presentation. n = 3 cells from 3 animals.

Europe PMC Funders Author Manuscripts

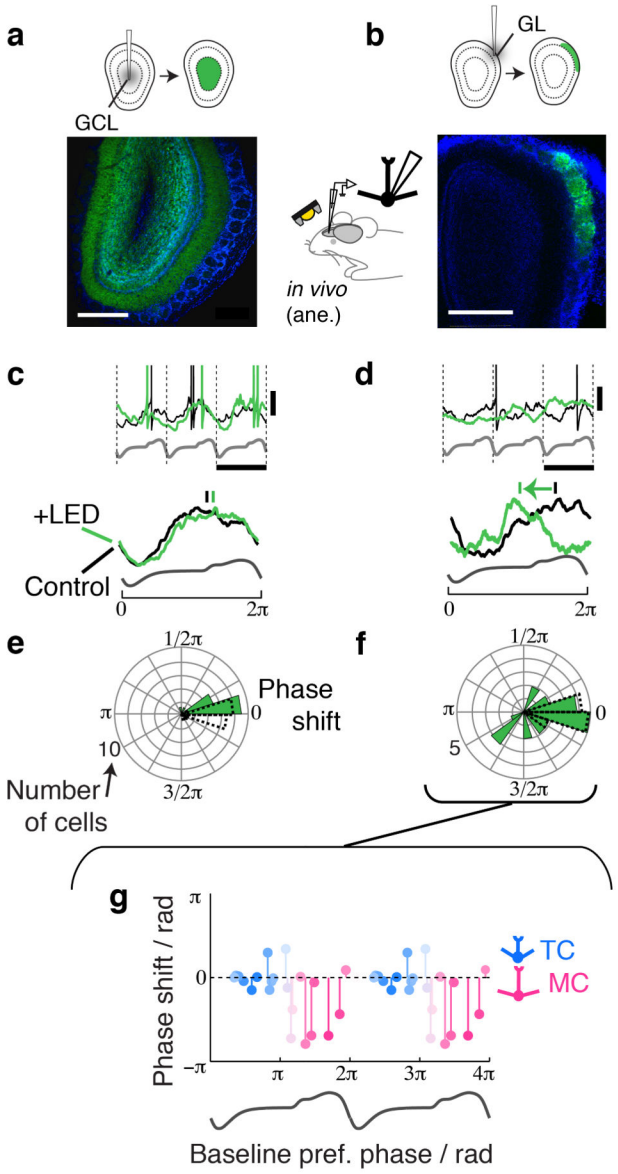

Figure 2. Glomerular layer inhibition structures the baseline theta rhythm

Layer selective optogenetic silencing of GABAergic neurons: AAV-FLEX-ArchT was injected into the GCL coordinates in the centre (**a**) or the GL coordinates superficially (**b**) of the OB. Green = GFP fluorescence and blue = DAPI staining. Scale bar = 0.4 mm. Inset illustrates the experimental configuration showing whole cell patch recordings made *in vivo* in anaesthetized Gad2-Cre or Vgat-Cre mice. (**c,e**) The effect of GC layer silencing on M/TC sniff-coupling; (**c**) Sniff-aligned, raw (top) Vm traces during control (black) and during LED presentation (green) from an example cell; nasal flow template is shown below (gray). Scale bars = 10 mV & 417.5 ms. (below) Sniff aligned, normalized average traces (from 165 sniff cycles for control and 60 cycles for LED conditions). Vertical bars above indicate the preferred phases for control (black) and LED (green) conditions. (**e**) Summary of phase shifts (φ_{LED}-φ_{Cont}) during GCL silencing as a polar histogram (green histogram). Baseline phase drift (φ_{Cont1}-φ_{Cont2}) is shown as dotted lines. n = 18 cells from 14 animals.

(**d,f**) Effect of GL silencing on M/TC sniff-coupling. (**d**) as (**c**), but for GL silencing. Scale bars = 10 mV & 352.5 ms (top). Average traces were from 77 cycles (control) and 24 cycles (LED). (**f**) Summary phase shift histogram for GL silencing (n = 23 cells from 16 animals). (**g**) Dependence of GL silencing-induced phase shift on the baseline preferred phase of the recorded M/TCs (n = 23 cells, same as in **f**). Color indicates the likelihood of the recorded cell being TCs (cyan) or MCs (pink) based on the preferred phase of sniff coupling (see Methods; ref[16]).

Europe PMC Funders Author Manuscripts

Europe PMC Funders Author Manuscripts

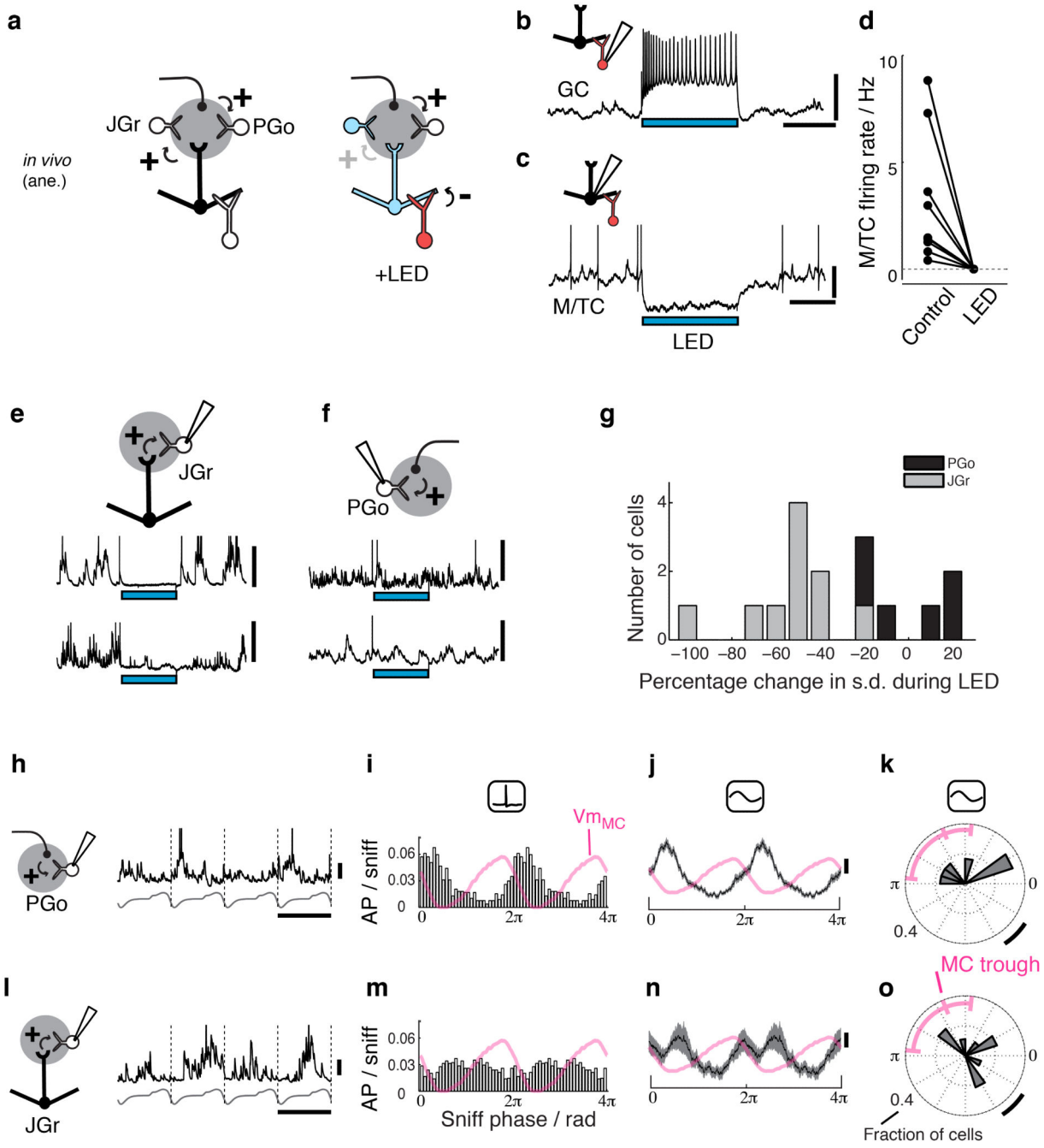

Figure 3. Sniff-coupling of distinct JGC populations

(**a-d**) Method used to distinguish putative PGo from other JGCs (JGr) *in vivo*. (**a**) Rationale for the method: (left) JGCs involved in the feedforward pathway (PGo) are predominantly driven by the olfactory nerve, while other types of JGCs (JGr) are significantly driven by M/TCs. (right) Activation of GCs via ChR2 suppresses M/TC activities, which in turn deprives excitatory drives to JGr cells, but not to PGo cells. (**b**) Example of an infected GC excited by ChR2 activation *in vivo* (blue bar = light presentation). (**c**) Example of hyperpolarization evoked in a M/TC during light presentation. (**d**) Summary of average M/TC firing rate for

control and light-on period. n = 8 cells from 5 animals. (**e**) Example whole cell recordings from two JGCs showing reduction in synaptic inputs during light presentation. Such cells are classified as JGr cells. (**f**) Examples of cells not showing reduction in synaptic inputs, classified as PGo cells. (**g**) Summary histogram of changes in Vm variance during light presentation. Cells with statistically significant changes in Vm variance are classified JGr cells (gray) while those without significant change are categorized as putative PGos. (**h-k**) Respiratory coupling properties of PGos. (**h**) Example Vm trace (black) from a PGo cell, aligned to respiratory rhythm. Nasal flow template is shown below (gray). Scale bar = 10 mV, 338 ms. (**i**) Histogram of AP phase from all PGo cells (n=6 cells from 6 animals), normalized by the number of sniff cycles analyzed. 284 ± 86 cycles per cell analyzed. Sniff-aligned average subthreshold Vm from morphologically identified MCs (n = 7 MCs; data reproduced from ref [16]) is overlaid for comparison (pink). Data is repeated over 2 cycles for illustration. (**j**) Sniff-aligned subthreshold Vm from all PGos (mean and 1 standard deviation shown). Pink trace is the same as in (**i**). (**k**) Summary polar histogram of preferred Vm phase of all PGos (gray), normalized by the total number of cells. Pink range indicates the preferred phase of MC hyperpolarization (ticks = 25, 50 & 75 percentiles, corresponding to 1.5, 2.0 & 3.0 radians). Scale bar = π/6 radians corresponding to 32.1 ms when calibrated for the average cycle lengths of all cells analyzed. (**l-o**) Respiratory coupling properties of JGr cells, as above. 412 ± 139 cycles per cell analysed. n = 10 JGr cells from 8 animals. Scale bar in (**l**) is 10 mV, 403 ms. Scale bar in (**o**) corresponds to 32.7 ms.

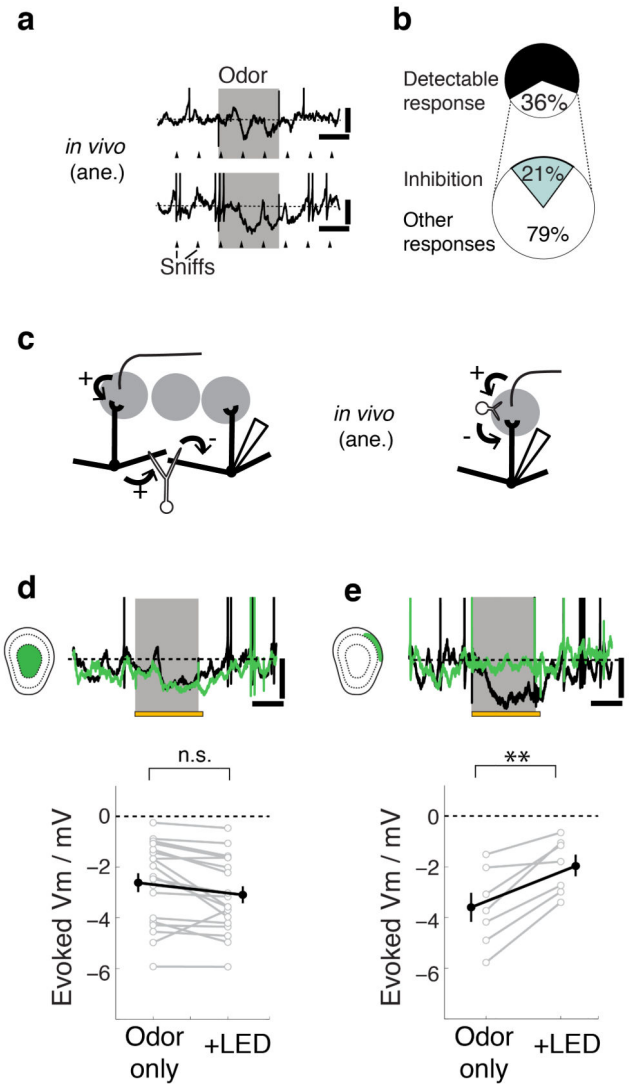

Figure 4. GL inhibition, rather than GC lateral inhibition, underlies slow odor-evoked inhibition

Odors presented to the animal often evoke sniff-coupled hyperpolarization in M/TCs as shown by two examples (**a**). Ticks represent the times of expirations peaks. Scale bars = 10 mV, 0.5 s. (**b**) For all cell-odor pairs (n = 205 pairs, 55 cells), 36% showed detectable responses, of which 21% are purely hyperpolarizing. (**c**) Two hypotheses for the source of the evoked inhibition: (left) M/TCs that receive excitatory input from neighbouring glomeruli activate GCs, which in turn give lateral inhibition to the recorded cell. (right) Feedforward inhibition within the glomerulus underlies evoked inhibition. (**d,e**) AAV-FLEX-ArchT was injected into the GCL and glomerular layer of Gad2-Cre or Vgat-Cre animals for layer-selective silencing as in Fig. 3. (**d**) Effect of GC silencing: Example Vm traces from a M/TC (top) during control (black) and during light presentation (green). Odor presentation (gray) was for 1 s and overlapped with light presentation (yellow) for the LED condition. Scale bars = 10 mV, 0.5 s. (below) Summary of evoked Vm during control (odor only) vs. during GC silencing (+LED). Mean ± s.e.m. shown. n = 19 cells from 13 animals.

Odors used = isoamylacetate, methylsalicylate and eugenol at 2-5% saturated vapor. (**e**) Effect of GL silencing: example traces & summary as in (**e**). n = 7 cells from 5 animals.

Europe PMC Funders Author Manuscripts

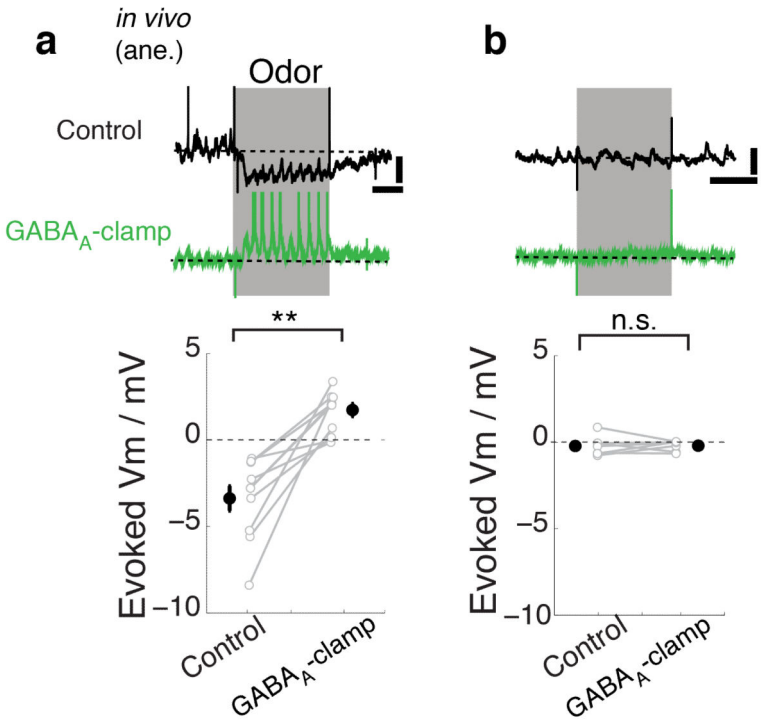

Figure 5. Feedforward circuit in the GL likely mediates the evoked inhibition

Pharmacological block of phasic $GABA_A$ activation ($GABA_A$-clamp; ref [16]) *in vivo*, in anesthetized C57/Bl6 mice by superfusion of gabazine (0.45 mM) and muscimol (2 mM) for at least 30 minutes. (**a**) Example traces from an M/T cell that showed odor evoked inhibition during control (black) and the effect of $GABA_A$-clamp (green) on this response. Dotted lines indicate the average Vm during baseline period. Scale bars = 10 mV, 0.5 s. (bottom) Summary of evoked potential during control and $GABA_A$-clamp conditions where odor evoked inhibition during control. Mean ± s.e.m. shown. n = 11 cell-odor pairs from 8 animals. (**b**) as in (**a**) but for cell-odor pairs where odor did not evoke detectable response during control. n = 7 cell-odor pairs from 3 animals. Odors used = isoamylacetate, eugenol, cinnamaldehyde, salicylaldelhyde, annisaldehyde. See also Supplementary Fig. 4.

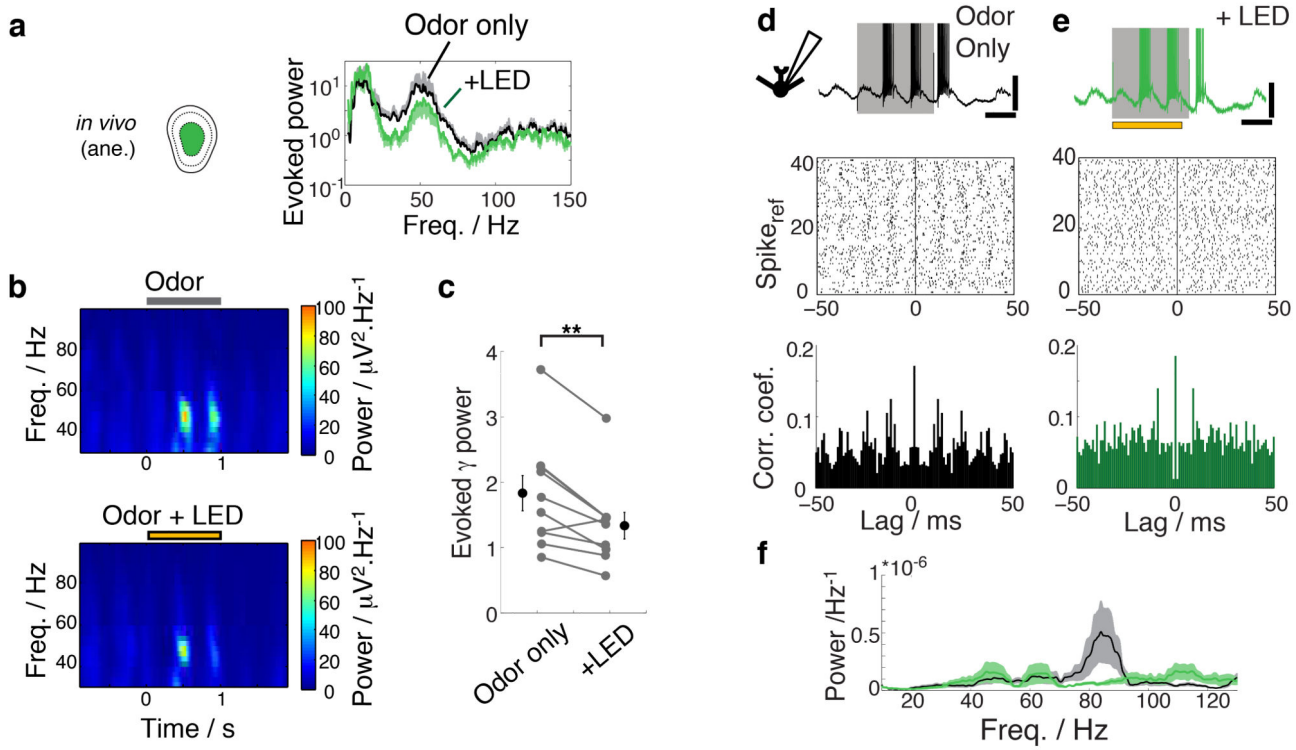

Figure 6. Granule cells coordinate neuronal activities on a fast timescale

(**a**) Spectral density estimate for odor period normalized by that for baseline period ("evoked power") averaged over all recordings (n = 10 recordings from 10 animals). Black = odor only, green = odor + LED. Mean and one standard deviation shown. Example spectrograms with odor only (top) and with additional GCL silencing (yellow bar; bottom). Hotter colors indicate greater power. Spectrograms are the average from 17 trials each. (**c**) Summary of evoked power averaged over gamma frequencies (40-100 Hz). Mean ± s.e.m. shown. (**d-f**) Gamma range activities on a single cell level. (**d**) Example of excitatory response evoked in an example TC (top). Gray bar indicates time of odor presentation. Scale bars = 20 mV, 0.4 s. (middle) Spike raster where timings of evoked APs are shown relative to a selected evoked spike ($spike_{ref}$) for 40 randomly chosen $spike_{ref}$. Spike autocorrelogram for this example cell is shown at the bottom (see methods). (**e**) as in (**d**) but with additional GCL silencing (yellow bar, top). Scale bars = 20 mV, 0.4 s. (**f**) Power spectra were obtained from the spike autocorrelogram for all TCs that showed excitatory responses (n = 9 cells from 8 animals) and averaged. Mean ± s.e.m are shown for odor only (black/gray) and with LED (green/pale green) conditions. Odors used = isoamylacetate, salicylaldehyde, eugenol, methylsalicylate and cinnamaldehyde at 2-5 % saturated vapor.

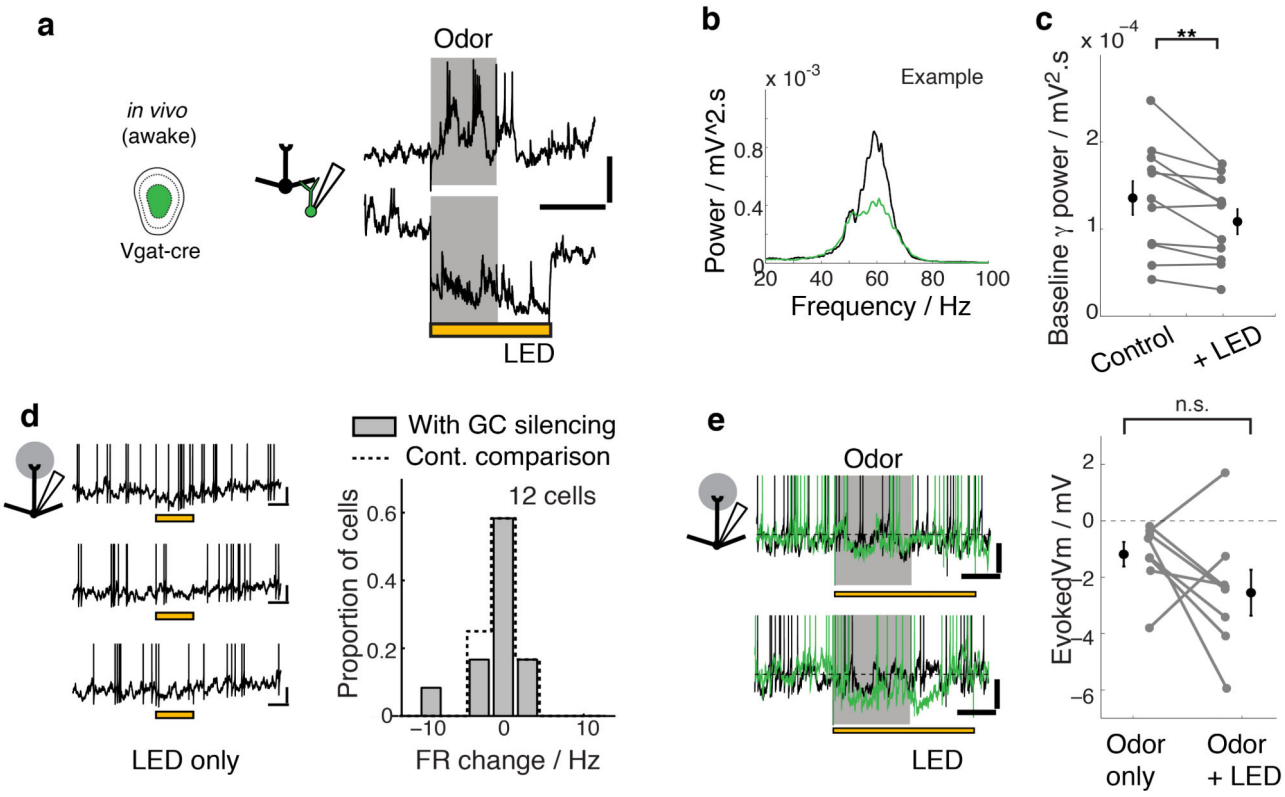

Figure 7. GCs contribute to fast, but not slow activities in awake animals

Whole cell and LFP recordings were made in the OB of awake, head-fixed Vgat-cre mice with AAV-FLEX-ArchT injection in the GCL ("GC silencing"). (**a**) Example whole cell recording from an infected GC that responded with AP discharge to stimulation with 5% of isoamylacetate. Odor-evoked responses under control conditions (top) and during light application (bottom). Scale bars, 20 mV, 1 s. (**b**) Spectral density estimates for an example LFP recording without external stimulus. Black = control, green = with LED. (**c**) Summary of average gamma power in the LFP (40-100 Hz). Mean ± s.e.m. shown. n = 11 recordings from 8 animals. (**d,e**) Effect of GC layer silencing on slow M/TC activities. (**d**) Effect of GC silencing on the baseline M/TC firing rates. Vm traces with repeated light presentations for an example cell (left). Scale bars = 10 mV, 0.5 s. Summary histogram of average firing rate change with light is shown on the right ($FR_{LED} - FR_{Control}$; n = 12 M/TCs from 5 animals). (right) Histogram shown with dotted line is for the baseline variability ($FR_{Control2} - FR_{Control1}$; see Methods). (**e**) Effect of GC silencing on odor-evoked inhibition. (left) Example recordings from 2 cells where an odor evoked hyperpolarization during control (black traces), and the effect of GCL silencing (green traces). Scale bars = 5 mV, 0.5 s. Evoked Vm are summarized on the right; mean ± s.e.m. shown. (n = 8 cell-odor pairs from 3 animals). Odors used = isoamylacetate, salicylaldehyde, eugenol, methylsalicylate, acetophenone and ethylbutyrate at 1-3 % saturated vapor.

Europe PMC Funders Author Manuscripts